European Journal of Computational Mechanics
Vol. 21, Nos. 3–6, June–December 2012, 351–364

Taylor & Francis
Taylor & Francis Group

Numerical modelling of sheet metal forming and crashworthiness of laminated steel structures using multi-layered solid-shell elements

S. Shiri[a], H. Naceur[a]* and J.M. Roelandt[b]

[a]*Lab. LAMIH, University of Valenciennes, Valenciennes, France;* [b]*Lab. ROBERVAL, University of Technology of Compiègne, Compiègne, France*

We present here a finite element (FE) model for the efficient modelling of deep drawing and crashworthiness simulation of multi-material structures. The multi-layered continuum FE is formulated in large strains with normal and transverse shear stresses to model effectively the behaviour of a wide variety of structures from very thin, thick and volumetric 3D. The FE model is implemented in LS-DYNA code, in its implicit and explicit formulations, using a 2×2 integration in the shell plane for each layer, respectively and an arbitrary number of integration points in thickness direction. Numerical examples are presented and compared to experimental measurements to demonstrate the effectiveness of the present FE model.

Nous présentons ici un modèle FE pour la modélisation efficace de l'emboutissage et du crash de structures multi-matériaux. Le modèle EF multicouches est formulé en grandes déformations avec prise en compte de la déformation transverse et des déformations de cisaillement ce qui permet de modéliser efficacement le comportement d'une grande variété de structures allant de très mince, à volumétrique. Le modèle FE est implémenté dans le code LS-DYNA, à la fois en statique implicite et en dynamique explicite, en utilisant une intégration 2x2 dans le plan moyen de chaque couche et un nombre arbitraire de points d'intégration dans le sens de l'épaisseur. Des exemples numériques sont présentés et comparés aux mesures expérimentales pour démontrer l'efficacité du modèle FE proposé.

Keywords: deep drawing; crash; multi-materials; large strains; solid-shell.

Mots-clés: emboutissage; crash; multi-matériaux; grandes déformations; solide-coque.

1. Introduction

The continuum elements are increasingly used for simulation of industrial applications such as forming and crashworthiness analysis. These elements can better describe the normal stresses in the thickness direction than classical thick shell elements where normal stress is zero since plane stress assumption is often used (Hannachi, Naceur, & Batoz, 2007). Moreover, continuum elements have only translational degrees of freedom, which reduce the complexity of rotational degrees of freedom. On the other hand, the total computation time needed by the use of such elements is reasonable when compared to standard brick 3D models (Shiri, Naceur, & Roelandt, 2009).

Sze and Ghali (1993) and Domissy, Bouabdallah, and Batoz (1995) are probably the first authors to suggest a solid-shell approach for the analysis of plates and shells. Since that time,

*Corresponding author. Email: hakim.naceur@univ-valenciennes.fr

ISSN 1779-7179 print/ISSN 1958-5829 online

http://dx.doi.org/10.1080/17797179.2012.714852
http://www.tandfonline.com

solid-shell concept has gained enormous contributions and models are continuously under improvements. Many recent works such as Harnau and Schweizerhof (2006), Hannachi et al. (2007), Quy and Matzenmiller (2008), Nguyen, Pham, Hogge, and Ponthot (2008), Shiri et al. (2009) and many others, who propose different techniques to carry out the general formulation of solid-shell finite element. They also deal with their application in the general structural mechanics with both linear and geometrical non-linear behaviour. However, they limit their validations to academic application such as plates, cylinders and spherical shells.

The objective of this work is the development of a numerical approach for the modelling of multi-layered structures and the identification of their behaviour in deep drawing and crashworthiness simulation. In order to achieve this goal, it was chosen to use a multi-layered multi-material solid-shell finite element in large strains with normal and transverse shear stress to model effectively the behaviour of complex structures containing a level of non-linearities (Shiri et al., 2009). As a first attempt, we present an efficient hexahedral solid-shell element formulation for analysis of large deformable multi-layered shell structures with non-linear materials, using the first-order equivalent single-layer approach. This model uses 2×2 integration in the shell plane for each layer and an arbitrary number of integration points in thickness direction. Thus, highly non-linear stress states over the sheet thickness can be incorporated in an efficient way. A particular attention will be given to the problems of numerical locking.

The element formulation and material model have been implemented into LS-DYNA commercial code (Hallquist, 2001) by means of the user-defined elements (UEL) interface. Numerical examples involving explicit dynamic analysis of multi-layered structures with both material and geometric non-linearities are presented and compared with experimental results to demonstrate the accuracy of the present methodology.

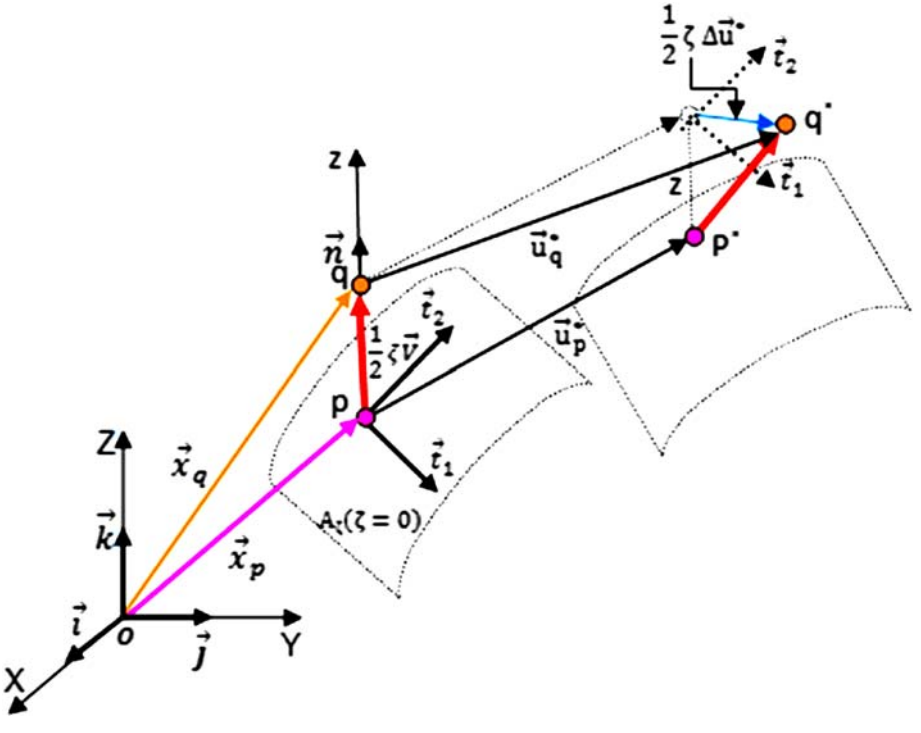

Figure 1. Kinematic description of the 3D shell.

2. FE formulation of the eight-node hexahedron

2.1. Kinematics of solid-shell model

In this section, the formulation of the eight-node solid-shell element is briefly recalled (for more details, see Hannachi et al., 2007). With respect to nodal designation, the coordinate vector $\mathbf{X}$ and displacement vector $\mathbf{U}_q$ of the element are (Figure 1)

$$\mathbf{x} = \mathbf{x}_0(\xi,\eta) + \frac{\zeta}{2}\,\mathbf{x}_n(\xi,\eta) = \sum_{i=1}^{4} N_i(\xi,\eta)\left(\frac{1-\zeta}{2}\,\mathbf{x}_i^- + \frac{1+\zeta}{2}\,\mathbf{x}_i^+\right) \tag{1}$$

$$\mathbf{u} = \mathbf{u}_0(\xi,\eta) + \frac{\zeta}{2}\,\mathbf{u}_n(\xi,\eta) = \sum_{i=1}^{4} N_i(\xi,\eta)\left(\frac{1-\zeta}{2}\,\mathbf{u}_i^- + \frac{1+\zeta}{2}\,\mathbf{u}_i^+\right) \tag{2}$$

where N_i are the 2D isoparametric Lagrangian interpolation functions, ξ, η and ζ are curvilinear coordinates, $\mathbf{x_i^-}$, $\mathbf{u}_i^-$ and $\mathbf{x_i^+}$, u_i^+ are, respectively, the coordinate and displacement vectors of the ith node on the bottom and top shell surfaces (Figure 1).

In this work, linear, isoparametric hex-shell elements are used with bilinear interpolation in membrane and linear interpolation in thickness direction. The displacement gradient in the cartesian framework is obtained from its image in the parametric description

$$\mathbf{L} = \mathbf{L}_\zeta\,\mathbf{F}_\zeta^{-1} \tag{3}$$

$\mathbf{L}_\zeta$ and $\mathbf{F}_\zeta$ are the displacement gradient tensor and the deformation gradient tensor, respectively, they are expressed in the parametric space, and are given by

$$\begin{aligned} \mathbf{L}_\zeta &= [\mathbf{u}_{,\xi} \vdots \mathbf{u}_{,\eta} \vdots \mathbf{u}_{,\zeta}] \\ \mathbf{F}_\zeta &= [\mathbf{a}_{1\zeta} \vdots \mathbf{a}_{2\zeta} \vdots \mathbf{a}_{3\zeta}] \end{aligned} \tag{4}$$

with the contravariant basis vectors $\mathbf{a}_{1\zeta} = \tilde{\mathbf{x}}_{,\xi} + \frac{1}{2}\zeta\,\mathbf{V}_{,\xi}$, $\mathbf{a}_{2\zeta} = \tilde{\mathbf{x}}_{,\eta} + \frac{1}{2}\zeta\,\mathbf{V}_{,\eta}$ and $\mathbf{a}_{3\zeta} = \frac{1}{2}\zeta\,\mathbf{V}$.

Cartesian components of the Green–Lagrange strain tensor $\mathbf{E}$ can be related to the curvilinear strain tensor $\mathbf{E}_t$ using the orthonormal transformation operator $\mathbf{Q} = [\mathbf{t}_{1\zeta} \vdots \mathbf{t}_{2\zeta} \vdots \mathbf{n}_\zeta]$, it can be also connected to the covariant basis $\mathbf{E}_\xi$, using

$$\mathbf{E}_t = \mathbf{Q}^T\,\mathbf{E}\,\mathbf{Q} \qquad \mathbf{E} = \mathbf{F}_\zeta^{-T}\,\mathbf{E}_\xi\,\mathbf{F}_\zeta^{-1} \tag{5}$$

Using Equation (5), one can obtain a direct relationship between curvilinear and the covariant strains:

$$\mathbf{E}_t = \mathbf{C}_\zeta^T\,\mathbf{E}_\xi\,\mathbf{C}_\zeta \tag{6}$$

with $\mathbf{C}_\zeta = \mathbf{F}_\zeta^{-1}\,\mathbf{Q}$. The covariant Green–Lagrange strain tensor is then given by

$$\mathbf{E}_\xi = \mathbf{F}_\zeta^T\,\mathbf{L}_\zeta + \mathbf{L}_\zeta^T\,\mathbf{F}_\zeta + \mathbf{L}_\zeta^T\,\mathbf{L}_\zeta \tag{7}$$

2.2. Weak formulation

In order to deal with the several lockings, we need to separate the expression of virtual internal work by uncoupling the membrane/bending, transverse/thickness and shearing (Hannachi et al., 2007).

$$W_{\text{int}} = \sum_{e=1}^{\text{nelt}} W_{\text{int}}^{\text{e}}; \qquad W_{\text{int}}^{e} = W_{\text{int}}^{\text{mb}} + W_{\text{int}}^{\text{tr}} + W_{\text{int}}^{\text{sh}} \tag{8}$$

$$W_{\text{int}}^{\text{mb}} = \int_{V^0} \delta\mathbf{E}_{\text{mb}}\, \mathbf{S}_{\text{mb}}\, dV = \delta\mathbf{u}^T\, \mathbf{f}_{\text{int}}^{\text{mb}}; \qquad \mathbf{f}_{\text{int}}^{\text{mb}} = \int_{V^0} \mathbf{B}_{\text{mb}}^T\, \mathbf{S}_{\text{mb}}\, dV \tag{9}$$

$$W_{\text{int}}^{\text{tr}} = \int_{V^0} \delta\mathbf{E}_{\text{tr}}\, \mathbf{S}_{\text{tr}}\, dV = \delta\mathbf{u}^T\, \mathbf{f}_{\text{int}}^{tr}; \qquad \mathbf{f}_{\text{int}}^{\text{tr}} = \int_{V^0} \mathbf{B}_{\text{tr}}^T\, \mathbf{S}_{\text{tr}}\, dV \tag{10}$$

$$W_{\text{int}}^{\text{sh}} = \int_{V^0} \delta\mathbf{E}_{\text{sh}}\, \mathbf{S}_{\text{sh}}\, dV = \delta\mathbf{u}^T\, \mathbf{f}_{\text{int}}^{\text{sh}}; \qquad \mathbf{f}_{\text{int}}^{\text{sh}} = \int_{V^0} \mathbf{B}_{\text{sh}}^T\, \mathbf{S}_{\text{sh}}\, dV \tag{11}$$

with $\mathbf{E}$, the Green–Lagrange strain tensor split into three components $\mathbf{E}_{\text{mb}} = <E_{11}\ E_{22}\ 2E_{12}>$, $\mathbf{E}_{\text{tr}} = <E_{11}\ E_{22}\ E_{33}>$, $\mathbf{E}_{\text{sh}} = <2E_{13}\ 2E_{23}>$. The second Piola-Kirchhoff stress tensor $\mathbf{S}$ is also decomposed into three parts $\mathbf{S}_{\text{mb}} = <S_{11}\ S_{22}\ S_{12}>$, $\mathbf{S}_{\text{tr}} = <S_{11}\ S_{22}\ S_{33}>$ and $\mathbf{S}_{\text{sh}} = <S_{13}\ S_{23}>$. The internal force vector on the element level is then given by

$$\mathbf{f}_{\text{int}}^{u} = \mathbf{f}_{\text{int}}^{\text{mb}} + \mathbf{f}_{\text{int}}^{\text{tr}} + \mathbf{f}_{\text{int}}^{\text{sh}} \tag{12}$$

A solid-shell element formulated using Equations (9)–(11) with standard integration based on a 2×2 Gauss scheme in the in-plane of the shell element will fail because of numerous locking phenomena.

2.2.1. Remedies for shear locking

An effective method of resolving shear locking is the assumed natural strain (ANS) method in which the natural transverse shear strains are sampled and then interpolated at some discrete element points with a specific order (Dvorkin & Bathe, 1984; Batoz & Dhatt, 1992).

The transverse shear strains $E_{\xi\zeta}$ and $E_{\eta\zeta}$ are calculated according to the average surface plan (ζ=0), assuming that they vary linearly (Equation (13)), and are functions of E_{ξ} and E_{η} at the mid-side points (see Figure 2(a)).

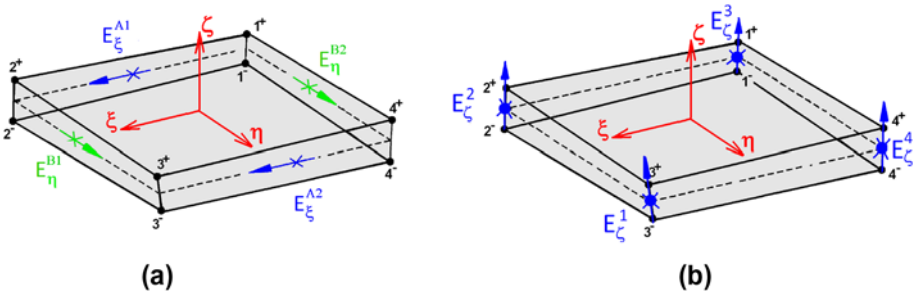

Figure 2. ANS method: (a) shear locking treatment and (b) trapezoidal locking treatment.

$$E^{\text{ANS}}_{\xi\zeta} = \frac{1-\eta}{2}\, E^{A1}_{\xi} + \frac{1+\eta}{2}\, E^{A2}_{\xi}; \quad E^{\text{ANS}}_{\eta\zeta} = \frac{1-\xi}{2}\, E^{B1}_{\eta} + \frac{1+\xi}{2}\, E^{B2}_{\eta} \tag{13}$$

The covariant components of the Green–Lagrange shear strain components are given by

$$\begin{aligned}
2\mathbf{E}^{A_1}_{\xi} &= \mathbf{a}_{1\zeta}\cdot\mathbf{u}_{,\zeta} + \mathbf{a}_{3\zeta}\cdot\mathbf{u}_{,\xi} + \mathbf{u}_{,\xi}\cdot\mathbf{u}_{,\zeta} \qquad \text{with } (\xi = 0, \eta = -1, \zeta = 0)\\
2\mathbf{E}^{A_2}_{\xi} &= \mathbf{a}_{1\zeta}\cdot\mathbf{u}_{,\zeta} + \mathbf{a}_{3\zeta}\cdot\mathbf{u}_{,\xi} + \mathbf{u}_{,\xi}\cdot\mathbf{u}_{,\zeta} \quad \text{with } (\xi = 0, \eta = +1, \zeta = 0)\\
2\mathbf{E}^{B_1}_{\eta} &= \mathbf{a}_{2\zeta}\cdot\mathbf{u}_{,\zeta} + \mathbf{a}_{3\zeta}\cdot\mathbf{u}_{,\eta} + \mathbf{u}_{,\eta}\cdot\mathbf{u}_{,\zeta} \qquad \text{with } (\xi = -1, \eta = 0, \zeta = 0)\\
2\mathbf{E}^{B_2}_{\eta} &= \mathbf{a}_{2\zeta}\cdot\mathbf{u}_{,\zeta} + \mathbf{a}_{3\zeta}\cdot\mathbf{u}_{,\eta} + \mathbf{u}_{,\eta}\cdot\mathbf{u}_{,\zeta} \qquad \text{with } (\xi = +1, \eta = 0, \zeta = 0)
\end{aligned} \tag{14}$$

In Equation (11), the shearing strains $\mathbf{E}_{\text{sh}}$ are substituted by the new ANSs $\mathbf{E}^{\text{ANS}}_{\text{sh}}$ given by Equation (13), thus the internal force vector due to shearing stresses takes the following expression:

$$\mathbf{f}^{\text{sh}}_{\text{int}} = \int_{V^0} \mathbf{B}^{\text{ANS}^T}_{\text{sh}}\, \mathbf{S}_{\text{sh}}\, dV \tag{15}$$

For the numerical evaluation of the integral in Equation (15), we use a 2×2 Gauss integration scheme in the element plane.

2.2.2. *Remedies for trapezoidal and volumetric locking*

Similar to shear locking, trapezoidal locking occurs when lower order elements such as eight-node hexahedral elements are used to model curved shells so that their cross-sections assume the trapezoidal shape. These excessive number of sampled thickness strains can be reduced by using a bilinear interpolation of the transverse normal strains sampled at the four corners of the element mid-surface (see Figure 2(b)), namely

$$E^{\text{ANS}}_{\zeta\zeta}(\xi,\eta) = \sum_{i=1}^{4} N_i(\xi,\eta)\, E_{\zeta}(\xi_i,\eta_i) \tag{16}$$

Volumetric (or material) locking is controlled by a material parameter, the Poisson ratio ν. Poisson's ratio coupling requires the thickness strain to be a linear function of ζ. Because our solid-shell element has only two layers, as a consequence the thickness strain does not vary with ζ thus the element fails in reproducing the plane-stress condition.

To overcome this problem, the transverse strain is enhanced, by introducing a linear variation in ζ, leading to the so-called enhanced assumed strains, namely

$$\tilde{E}^{\text{EAS}}_{\zeta\zeta}(\xi,\eta,\zeta) = E^{\text{ANS}}_{\zeta\zeta}(\xi,\eta) + \alpha\, \zeta\, t_{33} \tag{17}$$

where α represents an additional internal parameter which will be eliminated by special condensation technique on the element level, t_{33} is required for transformation to the local element coordinates. An additional condition has now to be satisfied locally, leading to the increment of the additional degrees of freedom.

$$\frac{\partial W_{\text{int}}}{\partial \mathbf{u}}\Delta\mathbf{u} + \frac{\partial W_{\text{int}}}{\partial \alpha}\Delta\alpha = -W_{\text{int}}(\mathbf{u},\alpha) \tag{18}$$

On the element level, the internal virtual work can now be computed with the compatible and the enhanced strains as in Equation (18).

$$W_{\text{int}} = \sum_{i=1}^{\text{nl}} \int_{\xi} \int_{\eta} \int_{\zeta_i}^{\zeta_{i+1}} (\delta \mathbf{E}_{\text{mb}}\, \mathbf{S}_{\text{mb}} + \delta \mathbf{E}_{\text{tr}}^{\text{EAS}}\, \mathbf{S}_{\text{tr}} + \delta \mathbf{E}_{\text{sh}}^{\text{ANS}}\, \mathbf{S}_{\text{sh}}) J d\xi d\eta d\zeta = \delta \mathbf{u}^T\, \mathbf{f}_{\text{int}}^e \tag{19}$$

nl is the number of layers and ζ_i is the transverse reference coordinate of the ith layer along the cross-section of the element.

In the context of modelling multi-layered composite materials using solid-shell elements, there exist two possibilities regarding the numerical implementation:

- *Case of one element per layer*: This is the easiest way for modelling the entire thickness of the structure using several elements (one element per layer) see Figure 3(a). In this case the numerical implementation of the model is straightforward and does not require any efforts in the implementation compared to the case of isotropic material modelling. The user has to provide the following basic properties:

  (1) Declaration of n groups of different elements in the FE mesh, the groups correspond to the n different layers constituting the laminate.
  (2) Provide the physical characteristics of the layer.

- *Case of several layers per element*: This second technique consists of stacking directly the different layers within the same element (see Figure 3(b)). Each FE is a stack of several layers, thus stress calculation and numerical integration of the internal force vector is carried out using the single-layer approach (identical to that commonly used for integration of plasticity). In the present investigation, this second method has been chosen and implemented because it is more general and more convenient since it requires only one element in the thickness of the structure (gain of computing time in the case of industrial applications).

In this case, the numerical implementation of the FE model requires some modifications of the stresses calculation and the integration of the internal force vector. For each FE, the user has to provide the following basic properties:

(1) Declaration of n groups of the different materials, the n groups correspond to the different layers constituting the multi-layer structure.

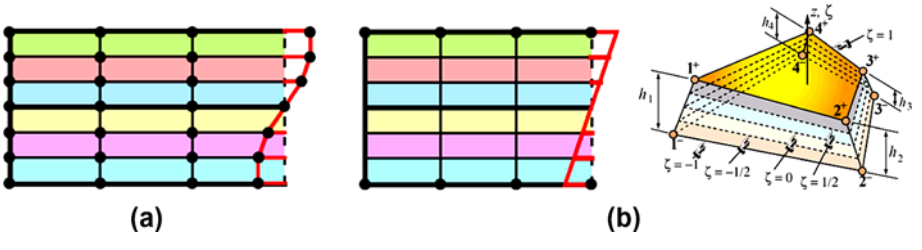

Figure 3. Composites modelling using solid-shell elements: (a) one element per layer and (b) several layers per element.

(2) Provide the physical characteristics for each material.
(3) Provide for each layer i, the thickness h^i (with $\sum_{i=1}^{n} h^i = h$ total thickness of the structure).

The numerical implementation is as follows, for example, the membrane/bending internal force vector, we have:

$$\mathbf{f}_{\text{int}}^{\text{mb}} = \int_A \left(\sum_{i=1}^{\text{nl}} \int_{z=-\frac{h^i}{2}}^{z=+\frac{h^i}{2}} \mathbf{B}_{\text{mb}}^T \, \mathbf{S}_{\text{mb}} dz \right) dA \tag{20}$$

where nl is the number of layers, h^i represents the layer thickness and h is the total thickness of the structure.

Equation (20) implies that for each layer of material, all operators are reported to the mid-plane of the layer then performs the numerical integration using Lobatto integration scheme with N points through the thickness. This operation is repeated for each layer, to cover the total thickness of the structure.

3. Numerical applications

3.1. *Bending of cantilever beam*

We consider in this very simple application, a benchmark for shear locking, well known from static analyses – the clamped cantilever beam with tip load – the geometrical and material parameters are given in Figure 4.

This benchmark is used to demonstrate the efficiency of the proposed solid-shell element compared to other classical solid elements regarding the shear locking phenomenon. To this end, the beam thickness is varied from $L/h = 1 - 1000$, which allow us to show the ability of the proposed solid-shell element, to model both 3D solids as well as thin shell structures without suffering from any shear locking effects.

The numerical solution of the beam bending problem was carried out using three different FE models: a 1-point integration hexahedron element (ELFORM01 of Ls-dyna code), a full integration hexahedron element (ELFORM02) and the proposed solid-shell FE model.

Table 1 shows the deflection solution obtained by the three models, function of the mesh refinement in both directions of the beam (length and thickness). First, we can observe from Table 1, that the proposed model gives very good results for the case of 3D solids even with few elements. When the ratio L/h increases, the structure becomes thinner, the proposed model keeps the same accuracy of solution, while the solution of the two other solid elements exhibit shear locking phenomenon.

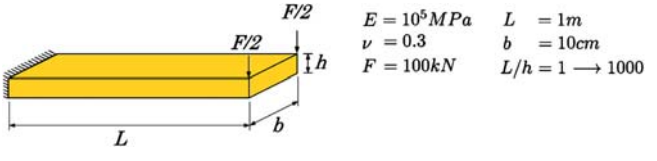

Figure 4. Test for shear locking; cantilever with tip load, varying $L/h = 1 - 1000$.

Table 1. Comparison of beam deflection obtained numerically to the analytical solution.

nb elem	ELFORM01	ELFORM02	Present model	Analytical
$L \times h \times b$		$L/h = 1$ (3D solid structure)		
$1 \times 1 \times 1$	4.245	.816	.733	1.000
$5 \times 5 \times 5$	1.162	1.005	1.013	1.000
$10 \times 10 \times 10$	1.097	1.010	1.009	1.000
$20 \times 20 \times 20$	1.040	.995	1.002	1.000
		$L/h = 10$ (thick shell structure)		
$1 \times 1 \times 1$	7.281	.026	.749	1.000
$10 \times 1 \times 1$	9.829	1.197	.995	1.000
$20 \times 2 \times 1$	1.283	.976	.997	1.000
$30 \times 3 \times 1$	1.106	.983	1.000	1.000
		$L/h = 100$ (thin shell structure)		
$1 \times 1 \times 1$	7.331	.000	.750	1.000
$10 \times 1 \times 1$	9.899	.026	.997	1.000
$20 \times 2 \times 1$	1.277	.095	.999	1.000
$30 \times 3 \times 1$	1.099	.189	1.000	1.000
		$L/h = 1000$ (very thin shell structure)		
$1 \times 1 \times 1$	7.322	.000	.749	1.000
$10 \times 1 \times 1$	9.900	.000	.998	1.000
$20 \times 2 \times 1$	1.275	.001	.999	1.000
$30 \times 3 \times 1$	1.098	.002	1.001	1.000

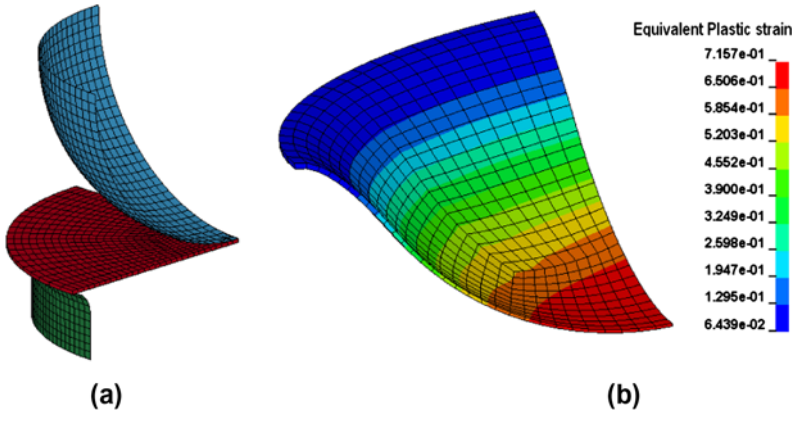

Figure 5. (a) Tools and blank mesh at the initial configuration and (b) effective plastic strain distribution.

3.2. *Wagoner deep drawing benchmark*

This benchmark was proposed by Lee, Wagoner, and Nakamachi (1990), it consists of the stretching analysis process of a thin sheet by a hemispherical punch. The final shape of the sheet is a hemisphere of radius 59.18 mm and depth 40 mm. All geometrical and material data can be found in Lee et al. (1990). Due to symmetry conditions, only a 1/4 of the blank is modelled, only 500 solid-shell elements are used for the discretisation of the 1/4 of blank, with only one solid-shell element in the thickness (Figure 5(a)). The deep drawing simulation

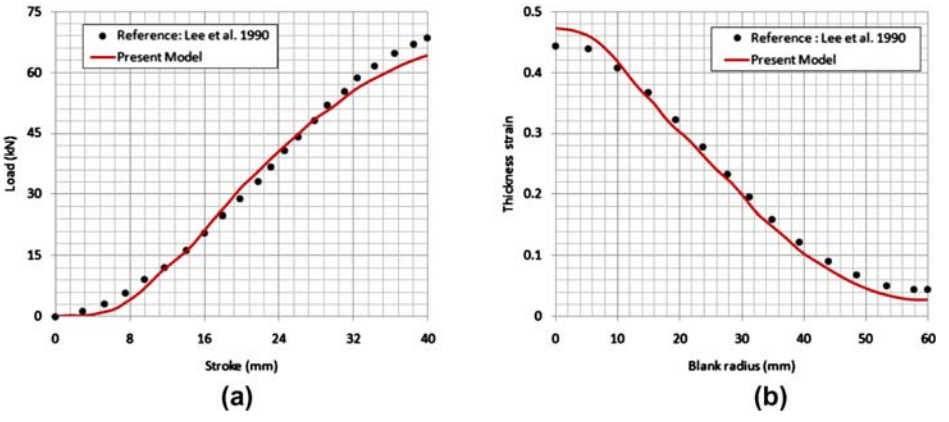

Figure 6. Principal results: (a) total punch force evolution and (b) thickness strain distribution along the radius.

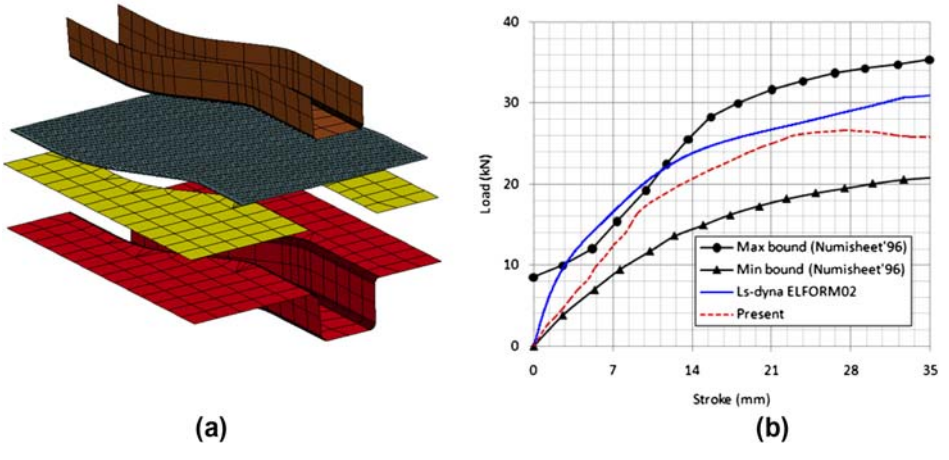

Figure 7. S-rail benchmark: (a) tools FE mesh and (b) punch force vs. stroke.

has been carried out using our model in its explicit dynamic version. Plastic strain distribution at the final deformed state is given in Figure 5(b).

Figure 6(a) shows the evolution of the total punch force in function of the stroke. As we can observe, the obtained force is in good agreement with the reference solution. Also the final thickness strain distribution along the initial radius is plotted in Figure 6(b) and compared to the reference solution as well as to the numerical solutions obtained using the Belytschko-Tsay (BT) shell elements and solid elements of Ls-dyna code. As we can observe, the present solid-shell element allows a good transverse strain estimation using only one element through the thickness.

3.3. S-rail deep drawing

The S-rail benchmark problem corresponds to one of the benchmarks proposed in NUMISHEET'96 (Lee, Kinzel, & Wagoner, 1996). The drawn part selected for this

benchmark contains combined bending and drawing zones, but the controlling of wrinkling and springback is a key problem.

The geometrical data of the tools can be found in Lee et al. (1996). Figure 7(a) shows the mesh used for the tools. The punch travel is 37 mm and the blank sheet of 1 mm thickness is made of *Al*6111 – *T*4. The material data used in this simulation are the same as the one used in the experiment by ALCOA (Young's modulus 69 GPa, Poisson ratio .3 and the hardening parameters $A = 368$ MPa, $B = 207$ MPa, and $C = 9.74$ MPa).

The deep drawing simulation is carried out using the implicit static version of the developed model using 6631 solid-shell elements with only one element in the thickness.

Figure 7(b) shows the punch force vs. the stroke, as we can notice that the obtained result from numerical simulation is situated within the two experimental border curves (extreme measurements), which indicated the effectiveness of the proposed FE model even if we use a quite coarse mesh.

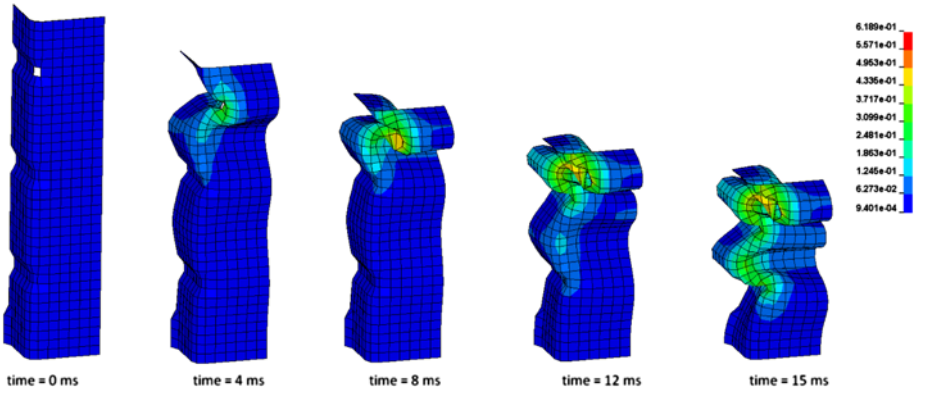

Figure 8. Plastic strain distribution – multiple configurations.

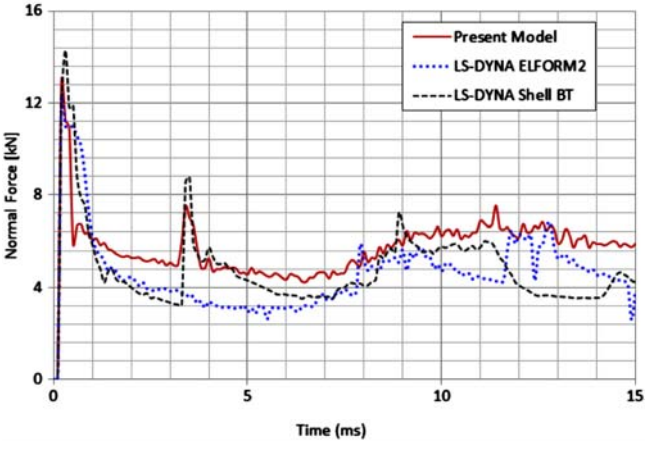

Figure 9. Impact force evolution vs. time.

3.4. *Tube crush impacted by a moving wall*

This application was introduced by Reid (2001), it consists of a tube of rectangular symmetrical cross-section which is impacted by a rigid wall of 800 kg with an initial speed of 8.94 m/s during 15 min.

All geometric and material data can be found in Reid (2001). Due to the symmetry, only 1/4 of the tube is modelled with only 467 solid-shell elements. Numerical simulations of crushing are performed using our model in its explicit dynamic version.

Figure 8 shows different deformed configurations with the equivalent plastic strain distribution at different time increments during lobes formation.

Figure 9 shows the normal impacting load, compared to those obtained by LS-DYNA classical models: B-T shell four-node shell element and the eight-node solid fully integrated. As we can notice, the obtained result matches those of LS-DYNA models, which indicates the efficiency of the proposed model.

3.5. *Draw bending of double curved Al/PP/Al sandwich sheet*

In this section, the draw-bending process of a sandwich sheet which includes two face sheets and a low-density core material (Figure 10) is investigated. This example is taken from the investigation described in Parsaa, Nasher al ahkamia, and Ettehadb (2010). The double curvature forming consists of bending the sheet with different curvatures at different directions as shown in Figure 10. The dimensions of the tools used in the numerical simulations are given in the above mentioned reference.

A three-ply sandwich sheet composed of aluminium alloy 3105 as face sheets and polypropylene as core material was considered as a blank sheet. The hardening behaviour of both aluminium and polypropylene sheet material was assumed to obey Hollomon law $\sigma_p = K\varepsilon_p^n$. The material properties of the used sandwich constituents are given in Table 2. Initial blank size was 100×100 mm. The thickness of the sandwich layers is .48 mm for the aluminium alloy and 1.04 mm for the polypropylene.

Within the free bending process, the workpiece originally resting on the die is undergoing bending by pressing the sandwich sheet with an upward moving punch travelling with a constant speed of 5 mm/s against the edges of the die. The maximum punch stroke was 24.5 mm.

The FE discretisation of the sandwich sheet in thickness direction is done using three different ways of modelling as shown in Figure 11.

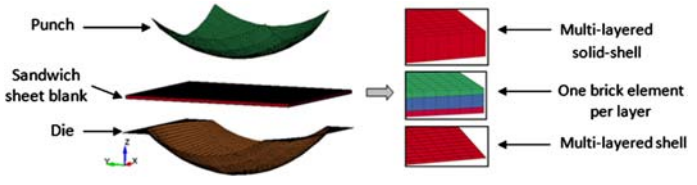

Figure 10. Schematics of the considered models for FEM analysis: different ways of modelling.

Table 2. Material properties of the used sandwich constituents in modelling.

Material	ρ (g cm^{-3})	E (GPa)	v	σ_y (MPa)	n	K (MPa)
Aluminium 3105	2.7	70	.33	27	.23	169
Polypropylene	1.0	15	.3	15	.14	39

- The introduced eight-*node layered solid-shell element* with only one element in the thickness direction.
- The standard *multi-layered BT shell element* with one integration point per layer.
- The standard *one-point hexahedrons* with three elements in thickness direction (one element per layer).

The effect of element size on computational results and CPU time was checked and elements size of 1×1 mm showed a reasonable result for all simulations. The evolution of the punch force as well as the final geometry of the sandwich sheet are investigated. The obtained results with the present multi-layered solid-shell model are compared to the experimental results reported in Parsaa et al. (2010). Also, the layered solid-shell solution was compared with the standard reduced integration hexahedron, multi-layered shell element of Ls-dyna solutions.

During bending, aluminium sheet layers and polymer materials with high radius of curvature are in the elastic–plastic state. Figure 11 compares the final geometries of deformed sand-

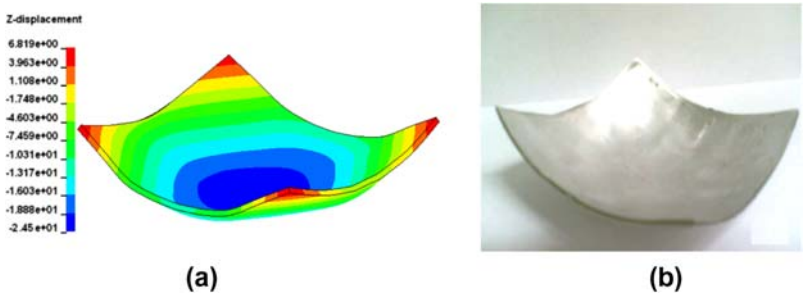

Figure 11. Final geometry: (a) numerical solution using proposed element and (b) experimentally formed sandwich sheet.

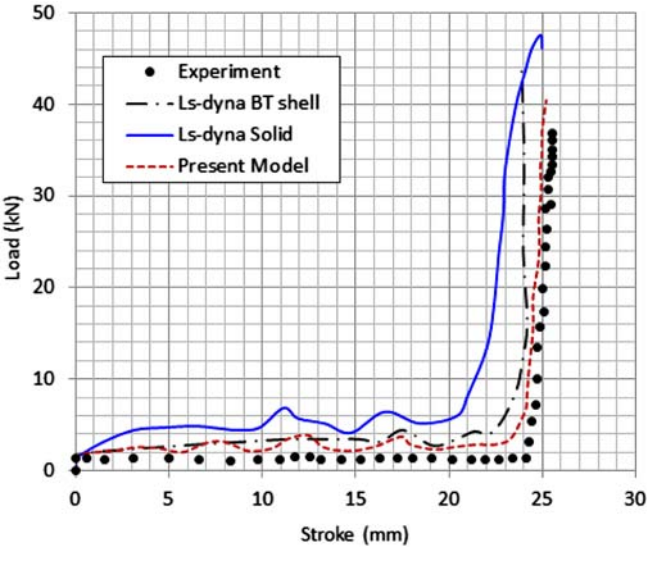

Figure 12. Total punch force evolution comparison numerical vs. experiments.

wich sheet predicted by numerical simulation using present solid-shell and obtained experimentally. As shown, there is a good agreement between experimental and simulation results.

The comparison between the simulation and the practical results from the test, in terms of punch load-displacement can be observed in Figure 12. As shown, the simulations curves follow the same trend predicted by experimental measurement.

The present result shows good performance of current layered solid-shell element which can represent different material layers' variable thickness inside one element with multiple integration points through the thickness. This may explain the differences between the numerical results, which are shown in Figure 11, especially for the zone of curves where the load rises sharply with the displacement and influenced by the developing and spreading of the plastic zone in the sandwich sheet.

4. Conclusion

In this paper, an efficient eight-node solid-shell element formulation for the analysis of multi-layered structures is presented. While the ANS method has been used in order to remedy to shear locking, the enhancement of transverse normal strain is adopted, thus full 3D anisotropic constitutive models are incorporated without resorting to the plane-stress assumption. The present formulation can predict the through-thickness effects with a high degree of accuracy. Due to the absence of rotational degrees of freedom as an alternative to the shell element, the present solid-shell element can be easily used in modelling shell structures. By defining several layers inside one layered element, number of elements through the thickness is remarkably reduced and significant computational time can be saved by avoiding the calculation of element stiffness matrix for each layer.

In fact, to model each ply with one solid element leads to undesirably big models and is impractical for large structures. Modelling sandwich structures with standard multi-layered shell elements, which neglect the normal stresses, will produce inaccurate results in transverse normal direction. Thus, present model which gives full 3D strain and stress field representation and combines the advantages of shell and solid elements, is a promising alternative for modelling layered structures.

References

Batoz, J.L., & Dhatt, G. (1992). *Modeling of structures by finite elements*, Vol. 3, Shells, Edition Hermès.

Domissy, E., Bouabdallah, S., & Batoz, J.L. (1995, September). *Formulation and evaluation of a solid finite element type for linear and nonlinear analysis of shells*. 12th French Congress of Mechanics, Strasbourg, France.

Dvorkin, E.N., & Bathe, K.J. (1984). A continuum mechanics based four-node shell element for general nonlinear analysis. *Engineering Computations, 1*, 77–88.

Hallquist, J.O. (2001). Ls-dyna keyword user manual. *Livermore Software Technology Corporation*.

Hannachi, M., Naceur, H., & Batoz, J.L., (2007). Continuum based solid-shell element modeling for the optimization of composite multilayered structures. *International Review of Mechanical Engineering, 1*(4), 150–163.

Harnau, M., & Schweizerhof, K. (2006). Artificial kinematics and simple stabilization of solid-shell elements occurring in highly constrained situations and applications in composite sheet forming simulation. *Finite Elements in Analysis and Design, 42*, 1097–1111.

Lee, J., Wagoner, R., & Nakamachi, E. (1990). *A benchmark test for sheet forming analysis* (NSF Engineering Research Center, Report No. ERC/NSMS-90). Ohio State University, Columbus.

Lee, J.K., Kinzel, G.L., & Wagoner, R.H. (1996). Numerical simulation of 3-D sheet metal forming processes: verification of simulations with experiments. In *Proceedings of the 3rd international conference on numerical simulation of sheet metal forming processes – verification of simulations with experiments, NUMISHEET'96*. 29 September - 3 October, Dearborn, Michigan.

Nguyen, N.H., Pham, V.N., Hogge, M., & Ponthot, J.P. (2008). An assumed natural strain technique for 2D solid-shell elements. In J.-F. Remacle and E. Dick (Eds.) *4th ICACME*, 26–28 May. Belgium: University of Liège.

Parsaa, M.H., Nasher al ahkamia, S., & Ettehadb, M. (2010). Experimental and finite element study on the springback of double curved aluminum/polypropylene/aluminum sandwich sheet. *Materials & Design, 319*, 4174–4183.

Quy, N.-D., & Matzenmiller, A. (2008). A solid-shell element with enhanced assumed strains for higher order shear deformations in laminates. *Technische Mechanik, 28*(3–4), 334–355.

Reid, J.D., (2001). Square crush tube with adaptivity, Ls-dyna examples manual (pp. 149–154). Livermore, California: Livermore Software Technology Corporation (LSTC).

Shiri, S., Naceur, H., Roelandt, J.M., Gacel, J.N., & Reynaert, A., (2009). Numerical modeling of stamping and crashworthiness of steel/polymer/steel structures using solid-shell element. In: E. Oñate and D.R.J. Owen (Eds), *10th International Conference on Computational Plasticity*, 5–7 September, Barcelona, Spain.

Sze, K.Y., & Ghali, A. (1993). An hexahedral element for plates, shells and beams by selective scaling. *International Journal for Numerical Methods in Engineering, 36*, 1519–1540.